PHILOSOPHICAL TRANSACTIONS OF THE ROYAL SOCIETY A MATHEMATICAL, PHYSICAL & ENGINEERING SCIENCES

Controlling and exploiting phases in multi-spin systems using electron spin resonance and nuclear magnetic resonance

Stephanie Simmons, Hua Wu and John J. L. Morton

Phil. Trans. R. Soc. A 2012 **370**, 4794-4809
doi: 10.1098/rsta.2011.0354

PHILOSOPHICAL TRANSACTIONS OF THE ROYAL SOCIETY A

CrossMark click for updates

Phil. Trans. R. Soc. A (2012) **370**, 4794–4809
doi:10.1098/rsta.2011.0354

Review

Controlling and exploiting phases in multi-spin systems using electron spin resonance and nuclear magnetic resonance

By Stephanie Simmons†, Hua Wu and John J. L. Morton*,†

Department of Materials, University of Oxford, Parks Road, Oxford OX1 3PH, UK

The phase of a superposition state is a quintessential characteristic that differentiates a quantum bit of information from a classical one. This phase can be manipulated dynamically or geometrically, and can be exploited to sensitively estimate Hamiltonian parameters, perform faithful quantum state tomography and encode quantum information into multiple modes of an ensemble. Here we discuss the methods that we have employed to manipulate and exploit the phase information of single-, two-, multi-qubit and multi-mode spin systems.

Keywords: magnetic resonance; spin qubits; phase gates; geometric phase; state tomography; multi-mode memory

1. Introduction

The power of quantum information processing (QIP) arises from the phase information contained in the processor [1]. In magnetic resonance, a spin qubit can acquire phase under various conditions: naturally through free evolution, dynamically (for example, through resonant applied pulses) and geometrically through path evolution. The acquired phase can be used to reveal details about the system environment through quantum metrology or about the composition of the quantum state itself through quantum tomography. If the applied phase is conditional on the state of another qubit, it is termed a controlled phase (CPHASE) operation—these are maximally entangling operations and allow for universal quantum computation. In this paper, we describe a family of phase manipulation techniques applied to electron and nuclear spin qubits, with a focus on geometric phase gates, and discuss their application in quantum metrology, tomography and multi-mode memories. This is not intended as a comprehensive review of the subject, but rather a summary of our work in this area.

*Author for correspondence (jjl.morton@ucl.ac.uk).
†Present address: London Centre for Nanotechnology, University College London, 17–19 Gordon Street, London WC1H 0AH, UK.

One contribution of 14 to a Theme Issue ‘Quantum information processing in NMR: theory and experiment’.

2. Single qubit phase manipulation

In both electron spin resonance (ESR) and nuclear magnetic resonance (NMR), microwave or radiofrequency (RF) pulses resonant with an allowed spin-flip transition are applied to create an oscillating magnetic field perpendicular to an applied static field (by convention, oriented along z). In the rotating frame of the spin, these pulses appear as static magnetic fields in the $\{X, Y\}$ plane, around which the spin precesses for the duration of the pulse. Thus, while rotations around the x- or y-axes (Pauli X or Y gates) can be performed directly through the application of a resonant pulse, Pauli Z gates (or phase gates) require a sequence of pulses.

There exist composite sequences made up of X and Y gates that perform dynamic Z rotations [2]. For example, a rotation of angle θ about the Z-axis can be performed with the sequence $(\pi/2)^X : (\theta)^Y : (\pi/2)^{-X}$, where the superscript on the rotation angle denotes the axis of rotation. Alternatively, one can operate in a different frame of reference [3,4] or apply off-resonant pulses and incorporate delays [5] to apply effective Z rotations. Each of these approaches have their limitations: pulses off-resonance sacrifice gate fidelity, delays increase the total gate time (and thus may suffer from additional decoherence), changing reference frames cannot be applied conditionally, and composite pulses can suffer from accumulated pulse errors [6]. An alternative method for accumulating phase invokes the spinor nature of the spin and accumulates phase geometrically through a closed-loop trajectory.

A quantum system that undergoes a cyclic evolution acquires a phase that depends on the geometry of the evolution path. This geometric phase is named Berry's phase when the evolution is adiabatic [7,8]. Berry's phase has been observed in different physical systems, including nuclear spins [9,10], electron spins in graphene [11] and Josephson junction devices [12,13]. Because it has been shown to be robust against certain parametric noises [14–16], the adiabatic Berry's phase is considered a promising approach to the phase manipulation of qubits and thus quantum gate operations in QIP [17,18]. In ESR, the adiabatic geometric phase gate based on Berry's phase provides a method for phase manipulation of electron spin qubits, which is potentially robust against inhomogeneities in the amplitude of the microwave field [19].

Adiabatic geometric phase gates can be realized in ESR by applying a microwave field near resonance that drives the evolution of the electron spins adiabatically around some closed-loop trajectory, as shown in figure 1 [20]. Consider an adiabatic evolution as follows: starting with the microwave detuned from resonance, the spin eigenstates are aligned along the Z-axis; then with the microwave slowly tuned onto resonance the instant eigenstates $|e_\pm(t)\rangle$ adiabatically follow the effective Hamiltonian and rotate into the $\{X, Y\}$ plane; then the phase of the microwave is swept while keeping the spin on-resonance so that the spin eigenstates rotate in the $\{X, Y\}$ plane to a certain angle ϕ; finally the microwave is tuned off-resonance again and the spin eigenstates rotate back to their original positions along the Z-axis. For an electron spin $\frac{1}{2}$, the geometric phase acquired by the spin eigenstates after such an evolution is half of the solid angle enclosed by the evolution path on the Bloch sphere, with the sign of the phase decided by the direction of the path. Therefore, the geometric phase acquired by a superposition state under this operation is $\gamma = \gamma_{|e_+\rangle} - \gamma_{|e_-\rangle} = \phi$. The

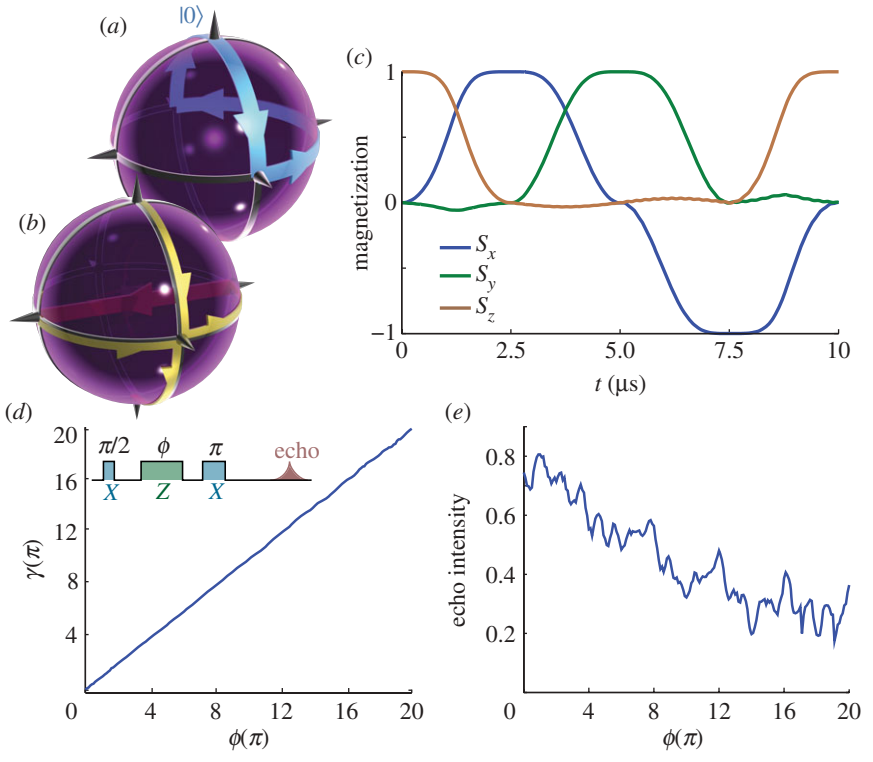

Figure 1. (*a*) Evolution of the spin eigenstate $|0\rangle$ as a result of (*b*) the effective magnetic field in the rotating frame. State $|1\rangle$ undergoes a similar trajectory, acquiring the opposite phase shift, creating an overall adiabatic geometric phase gate of $\phi = \pi$. (*c*) Simulated evolution of the spin magnetization of the initial state $|0\rangle$ during the adiabatic π phase gate. (*d*) Phase and (*e*) intensity of the spin echo signal measured after the adiabatic phase gates of $\phi = 0$ to 20π. The intensity is normalized against a Hahn echo detected following the same duration after the initializing $\pi/2$ pulse. (*d*, inset) Pulse sequence to apply and measure the adiabatic phase gates. (Online version in colour.)

dynamic phase of the spin eigenstates, on the other hand, can be eliminated by applying a π phase shift in the microwave in the middle of the adiabatic passage. By doing this, the instant spin eigenstates swap with each other and the dynamic phases acquired during the two halves of the adiabatic passage have opposite signs and therefore cancel each other out [21].

The dynamics of the electron spin during the adiabatic passage is determined by the effective Hamiltonian in the rotating frame of the resonance frequency ω_0:

$$H = \hbar \begin{pmatrix} 0 & \frac{1}{2} e^{i(\Delta t - \Gamma)} \Omega \\ \frac{1}{2} e^{-i(\Delta t - \Gamma)} \Omega & 0 \end{pmatrix}, \tag{2.1}$$

where $\Delta = \omega_{\mathrm{mw}} - \omega_0$ is the detuning of the microwave from resonance; Ω and Γ are the amplitude and phase of the microwave. There are many possible choices for the time-dependent frequency, amplitude and phase of the applied microwave

field to drive the adiabatic passage. An example is illustrated in figure 1*c*, which shows the simulated evolution of the spin magnetization during an adiabatic geometric phase gate with $\phi = \pi$, as illustrated in the Bloch sphere in figure 1*a*. The adiabaticity condition requires that the evolution of the system, and thus the variation of any Hamiltonian parameters, should be slow: taking the total length of the adiabatic passage to be τ, the adiabatic condition is equivalent to $\tau \gg \Delta^{-1}, \Omega^{-1}$.

In the experiment, the driving field of the adiabatic passage is realized via amplitude-, frequency- and phase-modulation of the applied microwave field. In order to measure the phase gate, a $(\pi/2)^X$ pulse is first applied to create a spin coherence in the $\{X, Y\}$ plane. This is followed by the adiabatic phase gate of angle ϕ, and a π^X pulse to refocus the inhomogeneity in the static magnetic field. The phase and intensity of the spin echo are obtained from the quadrature detection of the spin echo signal, with the former being a measurement of the mean phase shift applied to the spins and the latter a measurement of the spread in the phase across different spin packets. Figure 1*d*,*e* shows the results for $\phi = 0$ to 20π with a fixed phase ramping period. It can be seen that for a broad range of ϕ, the mean phase of the spin ensemble follows well the relation $\gamma = \phi$. The echo intensity, on the other hand, falls with increasing ϕ because $\dot{\phi}$ gets larger and the phase gate becomes less adiabatic, consistent with simulations. Having implemented the single qubit adiabatic geometric phase gate, further studies on the effectiveness and robustness of adiabatic phase gates under different conditions will be interesting, especially in comparison with the dynamic gate operations.

The principles behind geometric phase gates do not rely upon adiabaticity to work [20]. Closed-loop trajectories on a Bloch sphere can also be defined using fast qubit rotations, and the solid angle of these trajectories corresponds to an applied phase to each of the relevant eigenstates. The two eigentstates map out opposing directions during a closed-loop evolution and acquire the phase equal to half the solid angle of the closed trajectory [22,23]. Consequently, ignoring global phases, the net effect on those two eigenstates is a geometric Z gate whose phase is equal to the solid angle of the trajectory.

The precise form of the trajectory is flexible; however, the use of two π pulses along different axes in the $\{X, Y\}$ plane provides a simple implementation of a geometric Z gate. Given the ability to perform π rotations about the axis $\hat{N} = \cos(\theta)X + \sin(\theta)Y$, we can apply the following unitary:

$$\pi^{\cos(\theta)X+\sin(\theta)Y}(-\pi)^X = -\mathrm{i}(\cos(\theta)\sigma_X + \sin(\theta)\sigma_Y)(\mathrm{i}\sigma_X) \tag{2.2}$$

$$= \cos(\theta)\sigma_{\mathbb{I}} - \mathrm{i}\sin(\theta)\sigma_Z \tag{2.3}$$

$$= (2\theta)^Z, \tag{2.4}$$

where the superscript defines the axis of rotation, and $\sigma_{\mathbb{I},X,Y,Z}$ are the Pauli matrices. The solid angle mapped out by the closed loop defined by these two pulses is 2θ, and this trajectory can be seen in figure 2*a*. These and related controlled geometric Z gates have been experimentally demonstrated in NMR [22], ESR [24], with polarized photons in an interferometer [25] and superconducting systems [26].

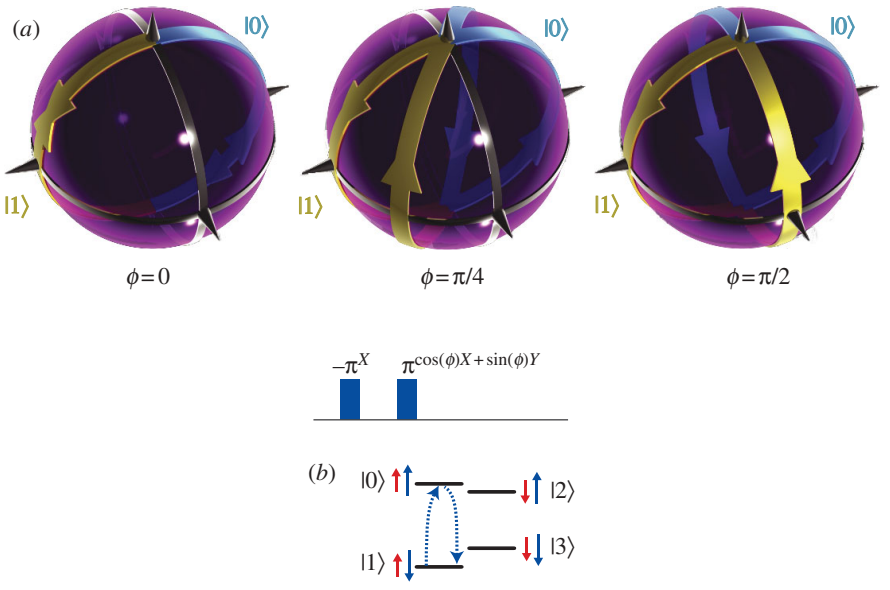

Figure 2. (*a*) Graphical representation of the solid angle mapped out by two π pulses about differing rotation axes in the $\{X, Y\}$ plane. A closed loop evolution imparts a geometric phase equal to half the solid angle defined by the path. The two eigenstates excited by the pulses acquire opposite phases, and consequently a Z phase gate is applied across them. (*b*) In systems of multiple coupled spins (e.g. blue, electron spin; red, nuclear spin), conditional phase gates can be applied by applying pulses that are selective on one transition. (Online version in colour.)

3. Two qubit phase manipulation

When these phase gates are applied to a two-level subsystem of a larger Hilbert space, the acquired phase on those eigenstates relative to the other undisturbed states amounts to a conditional Z gate. For example, take a coupled electron and nuclear spin, as shown in figure 2*b*. A conditional geometric Z gate of phase θ is applied by selectively exciting one of the electron spin transitions, resulting in the unitary

$$R^Z_{0,1} = \begin{pmatrix} \exp\left(\frac{\mathrm{i}\theta}{2}\right) & 0 & 0 & 0 \\ 0 & \exp\left(-\frac{\mathrm{i}\theta}{2}\right) & 0 & 0 \\ 0 & 0 & 1 & 0 \\ 0 & 0 & 0 & 1 \end{pmatrix}, \tag{3.1}$$

where the basis is $\{\Uparrow\uparrow, \Uparrow\downarrow, \Downarrow\uparrow, \Downarrow\downarrow\}$ and $\uparrow$ ($\Uparrow$) is the electron (nuclear) spin. Under this operation, coherences across the nuclear spin transitions also acquire a phase rotation. Indirect phase manipulations of this kind can be used to drive phase rotations to the nuclear spin on the much faster time scale of ESR pulses (tens of nanoseconds) [23]. This has been studied in the context of decoupling strategies, where microwave pulses applied to an electron spin qubit result in fast phase gates on a coupled nuclear spin qubit, which can dynamically decouple it from an applied RF field.

Such phase manipulations are useful for quantum state tomography. In systems where the experimental observable is a function of the population difference of two eigenstates (such as is the case for spins in NMR/ESR), all the eigenstate populations and coherent superpositions need be mapped onto this observable for readout. Pulse errors in this mapping process can lead to errors in the tomography, especially for those elements that require the most pulses to map them onto the observable. A more faithful measure of the density matrix involves using phase gates to uniquely label each coherence prior to readout [27,28]. Each coherence can be assigned a distinguishable time-varying phase through a sequence of phase operations [24], which corresponds to a diagonal unitary operator of the form

$$\begin{pmatrix} e^{i\theta_1} & 0 & 0 & \cdots \\ 0 & e^{i\theta_2} & 0 & \cdots \\ 0 & 0 & e^{i\theta_3} & \cdots \\ \vdots & \vdots & \vdots & \ddots \end{pmatrix} \tag{3.2}$$

such that $(\theta_a - \theta_b) \neq (\theta_c - \theta_d)$ for all distinct identifiers $\{a, b, c, d\}$ where $(a, b) \neq (c, d)$. As an example, for a coupled spin-$\frac{1}{2}$ spin-$\frac{1}{2}$ system, this condition can be satisfied with two conditional geometric phase rotations of the form described above. The operations $\theta^Z_{0,1}$ and $\eta^Z_{1,3}$ combine to form the unitary

$$\begin{pmatrix} e^{i\theta/2} & 0 & 0 & 0 \\ 0 & e^{-i\theta/2+i\eta/2} & 0 & 0 \\ 0 & 0 & 1 & 0 \\ 0 & 0 & 0 & e^{-i\eta/2} \end{pmatrix}. \tag{3.3}$$

The value of θ is incremented by $\delta\theta$ on each shot of the experiment, with an effective frequency of $\nu_\theta = 2\pi/\delta\theta$ (and similarly for η, $\delta\eta$ and ν_η). By applying this unitary prior to the readout, each coherence can be identified by an effective frequency: $\nu_\theta - \nu_\eta/2$ for a $|0\rangle\langle 1|$ coherence, $\nu_\eta/2$ for a $|2\rangle\langle 3|$ coherence, $\nu_\theta/2$ for a $|0\rangle\langle 2|$ coherence, $-\nu_\theta/2 + \nu_\eta$ for a $|1\rangle\langle 3|$ coherence, $-\nu_\theta/2 + \nu_\eta/2$ for a $|1\rangle\langle 2|$ coherence, and $\nu_\theta/2 + \nu_\eta/2$ for a $|0\rangle\langle 3|$ coherence. In this example, it is therefore important to choose ν_θ and ν_η such that $\nu_\theta \notin \{\pm\nu_\eta, \pm 2\nu_\eta, \pm\nu_\eta/2\}$ to ensure that the frequencies remain distinguishable. Quadrature measurement of these labelled coherences moved to the quantum observable allows us to discriminate between the resulting positive and negative frequencies.

The oscillations that this labelling process generates (figure 3) can be Fourier-transformed to reveal the presence of particular coherences, including their phase and amplitude. This process generalizes naturally to a large number of qubits, where the pulse overhead is linear in the number of qubits.

4. Multi-qubit phase manipulation

(*a*) *Fast CPHASE gates*

A conditional phase gate (or 'CPHASE' gate) is, like the controlled-NOT (CNOT), a maximally entangling quantum operation. As described earlier, in cases where some qubits are able to be manipulated quickly compared with other qubits (such as with an electron spin coupled to multiple nuclear spins), it can be

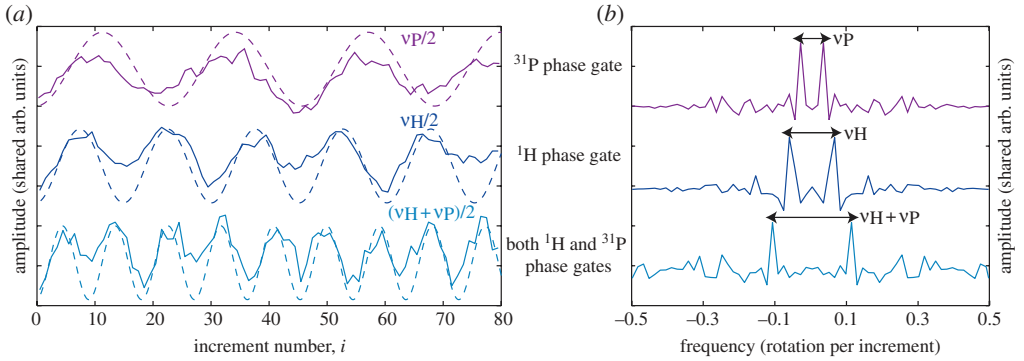

Figure 3. (*a*) A double quantum coherence responds to the sum of the phase rotations applied to its constituent eigenstates. This is illustrated using phosphorus and hydrogen nuclear spins in the DMHFP fullerene molecule [29]. Phase gates (whose angles are incremented) are applied to the either the phosphorus or hydrogen spins, or both, to observe the phase acquired by the double quantum coherence $(1/\sqrt{2})(|\uparrow\uparrow\rangle + |\downarrow\downarrow\rangle)$. Datasets are vertically offset for clarity, and the dashed curves correspond to the ideal result of these sequences given the known T_2 times for this system. (*b*) The Fourier transform reveals the resulting total phase rotation per increment which can be used to specifically label the double quantum coherence for tomography purposes. (Online version in colour.)

much faster to apply a controlled phase gate, rather than, say, CNOT. A suitably selective dynamic phase gate on the electron spin applies an indirect CPHASE between nuclear spins and provides a very fast entangling operation between nuclear spins [30–32].

We performed a demonstration of such a CPHASE operation on the C_{60} fullerene derivative dimethyl fullerene phosphine oxide or DMHFP, possessing two spin-active nuclei (^{31}P and ^{1}H) directly bonded to the C_{60} molecule. This molecule has a diamagnetic singlet ground state S_0, which can be photoexcited to populate the first excited singlet state S_1. This state undergoes intersystem crossing (ISC) to a long-lived triplet state that is paramagnetic. Preferential ISC rates and relaxation rates lead to unequal electron triplet populations, which creates some initial electron spin polarization. The two nuclear spins directly bonded to the fullerene cage couple to the photoexcited triplet, which can be used to drive fast, indirect CPHASE gates between them.

The Hamiltonian for this system is as follows:

$$\mathcal{H} = \mu_{\mathrm{B}} \boldsymbol{S}\mathbf{g}_{\mathbf{e}}\boldsymbol{B} + \boldsymbol{S}\mathbf{D}\boldsymbol{S} + \sum_{i=^{31}\mathrm{P},^{1}\mathrm{H}} \boldsymbol{S}\mathbf{A}(i)\boldsymbol{I}_i + JI_{1,z}I_{2,z} + \gamma_{i,n}\boldsymbol{I}_i \cdot \boldsymbol{B}, \qquad (4.1)$$

where $\boldsymbol{B}$ is the applied magnetic field, $\gamma_{i,n}$ the nuclear gyromagnetic ratio, $\mathbf{g}_{\mathbf{e}}$ the electron $\mathbf{g}_{\mathbf{e}}$-factor tensor, μ_{B} the Bohr magneton, $\mathbf{D}$ the zero-field splitting tensor for the $S = 1$ triplet state, $\mathbf{A}(i)$ the hyperfine coupling tensor between the triplet and the nuclear spins i and J the coupling between the nuclear spins. All terms involving $\boldsymbol{S}$ vanish in the electronic ground state.

The T_0 triplet subspace has four sub-levels corresponding to the four eigenstates of the phosphorus and hydrogen spins, which are split by the nuclear Zeeman interaction. NMR transitions within this subspace have narrow

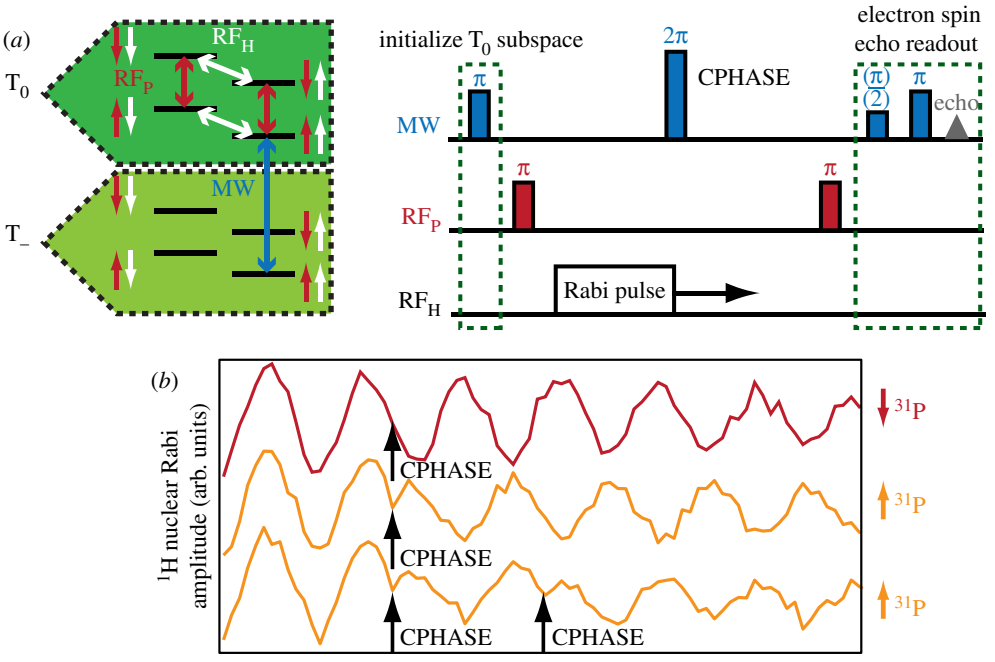

Figure 4. (*a*) Two levels of the photoexcited triplet state provide enough structure to perform fast indirect CPHASE operations on two nuclear spins. The T_0 sub-level is further split by the nuclear Zeeman term of the ^{1}H and ^{31}P spins, while the T_- triplet sub-level possesses further hyperfine splittings (6–11 MHz), allowing for microwave pulses selective upon a particular nuclear spin configuration. An applied 2π microwave pulse applies a phase of approximately π onto the particular nuclear eigenstate, which is equivalent to a CPHASE gate within the T_0 subspace. A pulse sequence to test this CPHASE gate applied during ^{1}H Rabi oscillations is shown, with optional phosphorus RF_P pulses to test its conditional behaviour. (*b*) Rabi oscillations respond to fast CPHASE gates conditional upon the phosphorus being spin-up (orange), and not spin-down (red). Multiple CPHASE operations can be applied, performing an ultrafast Z gate conditionally upon the ^{31}P spin state during the Rabi oscillations as shown. (Online version in colour.)

linewidths (less than or equal to 1 kHz), permitting high fidelity nuclear spin control compared with what can be achieved in the T_+ and T_- triplet subspace where NMR transitions are broadened by the anisotropic hyperfine coupling. The nuclear spin states within T_0 can be preferentially populated using a microwave π pulse tuned to a particular electron spin transition, which selects a particular nuclear configuration owing to the hyperfine coupling (figure 4*a*). At the end of the pulse sequence, an electron spin-echo amplitude measurement on this microwave transition provides a measurement of the nuclear spin configuration. A 2π pulse applied on the microwave transition imparts a π phase shift upon a particular nuclear spin eigenstate, resulting in a CPHASE gate on a time scale orders of magnitude faster than the direct nuclear coupling (approx. 3 kHz). The minimum duration of the CPHASE gate is limited only by the hyperfine coupling strength, which determines the maximum bandwidth of the microwave pulse. In this way, an entangling operation between nuclear spins on the time scale of hundreds of nanoseconds can be performed.

To illustrate how this phase gate can be applied to the individual nuclear spins, we applied 2π microwave pulses while driving nuclear Rabi oscillations on the ^{1}H spin, shown in figure 4*b*. Rabi oscillations on the complementary subspace are unaffected by the CPHASE operation, indicating that this gate is conditional. Similar behaviour is observed for Rabi oscillations on the ^{31}P nuclear spin. A CPHASE gate can be turned into a CNOT gate with leading and following RF $\pi/2$ pulses, and then used for quantum state tomography, as described earlier. This CPHASE gate can be scaled up to larger number of qubits, provided the microwave pulse can remain suitably selective.

(*b*) *Magnetic field sensing*

The density matrix tomography process discriminates between single and multiple quantum coherences by recording the frequency at which a coherence evolves. Multiple quantum coherences evolve as a weighted sum of the evolution frequencies of their constituent qubits' single quantum coherences [27]. This evolution can be a result of applied phase gates, but this evolution can also arise from the free evolution of the system. Some multiple quantum coherences acquire more phase per unit time than others, and this enhanced evolution allows for a more precise determination of the rate of phase acquisition [33–35]. It is through this mechanism that multiple quantum coherences can be used to determine Hamiltonian parameters more precisely than single quantum coherences, forming the basis for quantum metrology.

The time-evolution operator of an isolated two-level particle with a σ_Z Hamiltonian is given by

$$U(t) = \begin{pmatrix} \exp\left(-\dfrac{\mathrm{i}\zeta t}{2}\right) & 0 \\ 0 & \exp\left(\dfrac{\mathrm{i}\zeta t}{2}\right) \end{pmatrix}, \tag{4.2}$$

where ζ is a constant specific to the Hamiltonian and hence experimental environment. In this situation, a qubit in the state $\frac{1}{\sqrt{2}}(|0\rangle + |1\rangle)$ evolves according to $\frac{1}{\sqrt{2}}(|0\rangle + \exp(\mathrm{i}\zeta t)|1\rangle)$ (ignoring global phases). Observing this evolution allows for the extraction of ζ, which can yield information such as distance travelled [36,37], magnetic field magnitude [38] or the presence of a gravitational wave [39]. From the central limit theorem, the maximum precision of such a measurement taken over many averages (the standard deviation of measured values of ζ) scales as $\Delta/\sqrt{NR}(|\lambda_1 - \lambda_0|)$ for N the number of copies of probe particles, Δ^2 the variance of the measurement for each probe per unit time, $\lambda_{0,1}$ the Hamiltonian's eigenvalues and R the number of measurement repetitions [40]. This $1/\sqrt{N}$ scaling is known as the 'standard quantum limit' scaling [41].

The multiple quantum coherence $\frac{1}{\sqrt{2}}(|000...000\rangle + |111...111\rangle)$ with N identical qubits evolves over time as $\frac{1}{\sqrt{2}}(|000...000\rangle + \exp(\mathrm{i}N\zeta t)|111...111\rangle)$ [42]. This means that the relative phase of such a state evolves N times more quickly when compared with a solitary single quantum coherence. The maximum precision of such a measurement scales as $\Delta/N\sqrt{R}(|\lambda_1 - \lambda_0|)$ for N qubits [40]. This is

known as 'Heisenberg scaling', meaning that such sensitivities scale alongside the physical limits allowed by the uncertainty principle [43], recovering the time–energy uncertainty relation in the event that $\Delta = \hbar/2$. It therefore appears as if large states such as $\frac{1}{\sqrt{2}}(|000...000\rangle + |111...111\rangle)$, referred to as 'NOON' [33], 'GHZ' [42] or 'Schrödinger cat' [3] states, could be a powerful resource for enhancing sensors. In an optical environment, entanglement-enhanced sensors have been applied to interferometry [33], where slight changes in a path length were discerned more sensitively with a four-photon entangled state over that of four lone photon qubits.

To quickly generate large states such as $\frac{1}{\sqrt{2}}(|000...000\rangle + |111...111\rangle)$, it is advantageous to choose quantum systems with a high degree of coupling symmetry. With this in mind, we investigated molecules that possess nuclear spins in a *star topology*: a central spin-active nucleus (labelled A) distinct from, and coupled to, many magnetically equivalent spin-active nuclei (labelled B). The magnetic equivalence of the B nuclei permits the simultaneous addressing of all of them, streamlining the spin-NOON state creation. Examples of such star-topology molecules include the 9 (hydrogen) +1 (phosphorus) spin trimethylphosphate [44], 12+1 spin tetramethylsilane (TMS) [45] and 27+1 spin tris-(trimethylsilyl)phosphine.

To generate a NOON state with a star topology from the input pure state $|0\rangle^A|000...000\rangle^B$, one applies a coherence-generating $(\pi/2)^Y$ pulse on the centre spin A transforming the state into $\frac{1}{\sqrt{2}}(|0\rangle^A + |1\rangle^A)|000...000\rangle^B$, followed by a CNOT gate conditional upon A. The NOON state is left free to measure the magnetic field for a time τ, resulting in a state $\frac{1}{\sqrt{2}}(|0\rangle^A|000...000\rangle^B + \exp(\mathrm{i}N\zeta\tau)|1\rangle^A|111...111\rangle^B)$. To read out this phase, a reversal of the previous CNOT maps the acquired phase onto a coherence on spin A for readout, according to the state $\frac{1}{\sqrt{2}}(|0\rangle^A + \exp(\mathrm{i}N\zeta\tau)|1\rangle^A)|000...000\rangle^B)$. Observed in a magnetic resonance spectrum, such a sensor based on a pure initial state produces a single coherence (a single peak in the spectrum of spin A), whose phase evolves at a rate of $N\zeta$.

Although elegant in its experimental simplicity, liquid-state NMR generally deals with heavily mixed states. Without a pseudopure preparation of the state, a $(\pi/2)_A^Y$ pulse applied to a thermal state generates $N+1$ spectral peaks, separated in frequency by the J-coupling J^{AB}, corresponding to the thermal (roughly binomial) distribution of up and down spins of the coupled B nuclei. We can assign a number, ℓ, to each of these lines corresponding to their 'lopsidedness', that is $\ell = u - d$ where u and d are the number of intramolecular up and down B spins, respectively. The absolute value of ℓ corresponds to the degree of the corresponding multiple quantum coherence; $\ell = -3$ is a triple quantum coherence and so on.

One option is to apply pseudopure state preparation, which would behave as a pure initial state but with much lower amplitude owing to the pseudopure preparation sequence. The alternative of post-selecting the desired peak offers benefits. In addition to being computationally equivalent upon the peak of interest, the readout signal is stronger and the sequence time is shorter. A crucial advantage of this approach uses the fact that the other peaks also pick-up phase, proportional to their lopsidedness, and in most cases this is also beyond the scaling

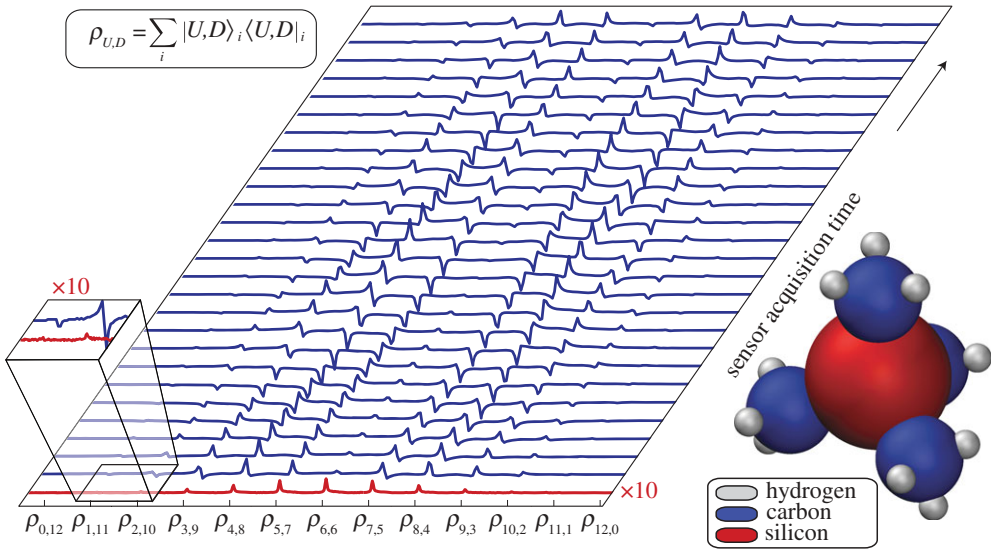

Figure 5. The ^{29}Si spin-echo NMR spectrum of TMS (shown right) is split into 13 peaks by coupling to the 12 magnetically equivalent ^{1}H spins, whose intensities follow a binomial distribution (bottom red trace, amplified 10-fold). Each peak can be labelled by the 'lopsidedness' ℓ: the difference between the number of coupled up and down ^{1}H spins. Each ℓ state can be used to form a corresponding many-some, some-many (MSSM) state suitable for magnetic field sensing, where the rate of acquired phase scales with ℓ, shown in the blue traces. A leading CNOT gate can amplify the overall signal by γ_R as well as linearly with ℓ. This improves the scaling of the sensor's weighted sensitivity beyond the scaling of the standard quantum limit. (Online version in colour.)

of the standard quantum limit. Thus, in general, the sensing sequence uses states that are not quite NOON states, and it is for this reason the term 'MSSM' was introduced [44] to describe these states (figure 5).

In the limit of large N, the weighted sum of these sensitivities is greater than that of an equivalent number of isolated spins, by only a small constant factor, and in both cases the sensitivity scales according to $1/\sqrt{N}$. This can be improved by adding an additional preparation stage to the sequence with a CNOT gate on the B spins controlled on the state of the central spin A. This multi-qubit version of the INEPT sequence [46] leads to an amplification of the signal from each peak according to $1 + \gamma_R \ell$, where $\gamma_R = \gamma_B/\gamma_A$ is the ratio of gyromagnetic ratios of the two species [45]. The lines with the greatest magnetic field sensitivity are therefore the most amplified by this sequence, and the weighted sensitivity now outperforms the scaling of the standard quantum limit [47,48] to $1/N^{3/4}$ even with the low nuclear polarization in the liquid-state NMR environment.

These metrology sequences are limited to relatively homogeneous spin environments, where the phase evolution is shared across the ensemble. In contrast, an excitation of a spin ensemble in an inhomogeneous environment, such as that provided by a magnetic field gradient, acquires phase non-uniformly as a mode across the ensemble. This encoded phase information can be recovered as a spin-echo allowing for a multi-mode quantum phase memory.

5. Multi-mode phase encoding

The phase of a collective excitation across an ensemble, created over different spatial [49] or frequency [50] components of the ensemble, can be used to define a mode suitable to store quantum information. A spatially distributed phase mode can be created with an inhomogeneous external field and on-demand retrieval of the stored information can be realized though methods based on controlled reversible inhomogeneous broadening [51–54]. A large number of spins in an ensemble provides a resource for extending this to the storage of many qubits using multi-mode phase encoding [55–58].

A qubit stored in an ensemble of N spins in the form of a singly excited collective state is written as $|\psi_0\rangle_{\rm ens} = \frac{1}{\sqrt{N}} \sum_j |g_1 \cdots e_j \cdots g_N\rangle$. In ESR, when a magnetic field gradient G is applied on top of the homogeneous static field along the Z axis (neglecting the random inhomogeneities of the static field), the field gradient induces an inhomogeneous phase evolution of the spins at different locations and the singly excited collective state becomes $|\psi_k\rangle_{\rm ens} = \frac{1}{\sqrt{N}} \sum_j {\rm e}^{{\rm i}k\cdot Z_j} |g_1 \cdots e_j \cdots g_N\rangle$, where the wavevector k of the spin-wave excitation is defined by $k = (\mu_0 g_e/\hbar) \int G \, {\rm d}t$. Each of the spatially distributed collective phase modes is therefore characterized by a specific wavevector k. Two phase modes $|\psi_{k_1}\rangle, |\psi_{k_2}\rangle$ are orthogonal if $\langle\psi_{k_1}|\psi_{k_2}\rangle = \frac{1}{N} \sum_j {\rm e}^{{\rm i}(k_2-k_1)z_j} = 0$, and for large N, the orthogonality relation is always satisfied for any $k_1 \neq k_2$.

Mutually orthogonal phase modes are independent and can evolve without causing any crosstalk between each other, and the only phase mode coupled to the microwave field is the $k = 0$ mode. Therefore, any phase mode orthogonal to the $k = 0$ mode can be used for storing one qubit. In principle, the number of qubits that can be stored simultaneously in the orthogonal phase modes of the ensemble is limited by $\sqrt{N}$. This large storage capacity is an important advantage of the multi-mode phase encoding in an ensemble-based quantum memory.

Qubits can be read and written using the $k = 0$ mode, whereas during the storage period the qubits are moved to other, orthogonal, phase modes that are decoupled from the microwave cavity. Because a negative field gradient is equivalent to a positive field gradient of the same amplitude applied after a π rotation of all the spins, the retrieval of a qubit encoded in a certain phase mode can be realized with a π pulse followed by the same field gradient that creates the same phase mode. The deterministic storage of a qubit represented by a microwave photon requires strong coupling between the cavity and spin ensemble, which can be achieved using various types of resonator [59–61]. We can explore such methods, even outside of this strong-coupling or single-photon limit, using weak microwave pulses. Figure 6*a* shows the encoding of eight qubits represented by weak microwave pulses in an ensemble of phosphorus donor spins in silicon. A constant field gradient is applied during the whole pulse sequence. Before the π pulse at $t = 50\,\mu$s, the eight weak excitations, which are 8 ns microwave pulses corresponding to a tipping angle of approximately 0.02π, are encoded into eight different phase modes by the field gradient; after the π pulse, the field gradient brings the eight phase modes back to the $k = 0$ mode and eight spin echoes are observed indicating the retrieval of the encoded qubits.

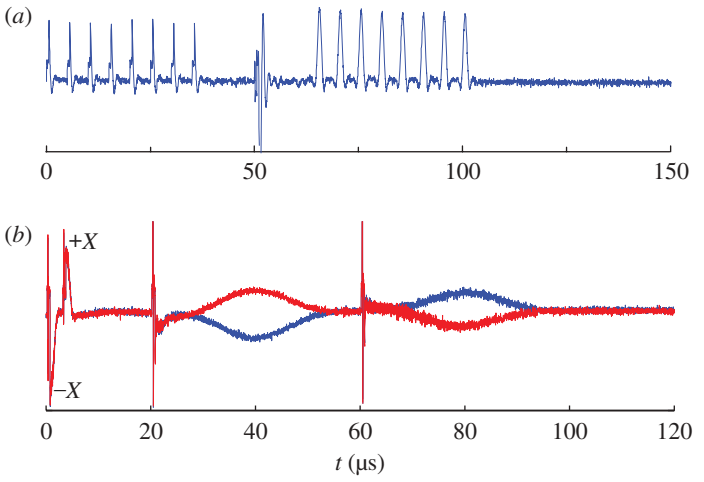

Figure 6. (*a*) Eight weak microwave pulses are applied to a sample of P-doped Si, resulting in weak excitations of the spin ensemble. These separate excitations are encoded in different collective phase modes using a constant field gradient, and later retrieved following a π pulse. (*b*) Independent readout of two microwave spin excitations of different phases. Blue trace: the pulse in $-X$ is read out before the one in $+X$; red trace: the pulse in $-X$ is read out after the one in $+X$. (Online version in colour.)

The orthogonality of the phase modes ensures that different modes can be addressed separately, meaning that the on-demand readout can be realized for each stored qubit independently. The key procedure is to bring the particular phase mode to $k = 0$ mode for readout at the required moment by applying an appropriate field gradient. Figure 6*b* demonstrates the independent on-demand readout of two microwave excitations, using pulsed field gradients in an ensemble of N@C_{60} molecules. The qubits are represented by two weak microwave pulses of 18 ns with phase oriented along $-X$ and $+X$, and the echoes in $-X$ or $+X$ indicate the retrieval of the corresponding qubit. The pulsed field gradients are controlled by current pulses through a pair of anti-Helmholtz coils placed around the resonator. A gradient pulse of 1.3 μs is applied after each microwave pulse to bring the first (second) microwave pulse into an orthogonal phase mode $2k_0$ (k_0); after the refocusing π pulse, applying two (one) gradient pulses of the same length and intensity brings the first (second) microwave pulse back to the $k = 0$ mode, and the spin echo of the corresponding microwave pulse is observed. The same principle also applies to multiple qubits. Therefore, the phase-encoded spin ensemble constitutes a random-access quantum memory. Such a multi-mode quantum memory is an important element for the hybrid quantum processor [62–64] where the long-lived spin ensemble is coupled to a superconducting qubit via a transmission line cavity [60,61,65].

6. Summary

We have described quantum control of the phase of electron and nuclear spin states by NMR and ESR, ranging from individual spins, coupled spins and

long-range collective states in spin ensembles. Both adiabatic and dynamic approaches can be used to apply phase gates, with the former offering some advantages in terms of gate robustness. We have also described potential applications that rely on phase control in spin ensembles, including density matrix tomography, (pseudo-)entanglement enhanced magnetometry based on nuclear spins and multi-mode microwave memories using electron spins.

We gratefully acknowledge helpful discussions with Vasileia Filidou, Erik Gauger, Mikko Möttönen, Jonathan Jones, Steve Karlen, Harry Anderson, Arzhang Ardavan, Andrew Briggs, Richard George and Simon Benjamin. We thank EPSRC for supporting this work through CAESR (EP/D048559/1), and acknowledge support from the Clarendon Fund, KCWong Education Foundation, Hitachi Cambridge Laboratory, St John's College Oxford and the Royal Society.

References

1 Jozsa, R. & Linden, N. 2003 On the role of entanglement in quantum-computational speed-up. *Proc. R. Soc. Lond. A* **459**, 2011–2032. (doi:10.1098/rspa.2002.1097)
2 Freeman, R., Frenkiel, T. & Levitt, M. 1981 Composite *Z* pulses. *J. Magn. Res.* **44**, 409–412. (doi:10.1016/0022-2364(81)90181-5)
3 Knill, E., Laflamme, R., Martinez, R. & Tseng, C.-H. 2000 An algorithmic benchmark for quantum information processing. *Nature* **404**, 368–370. (doi:10.1038/35006012)
4 Jones, J. A. 2001 NMR quantum computation. *Prog. Nucl. Magn. Reson. Spec.* **38**, 325–360. (doi:10.1016/S0079-6565(00)00033-9)
5 Emsley, L. & Bodenhausen, G. 1990 Phase shifts induced by transient Bloch–Siegert effects in NMR. *Chem. Phys. Lett.* **168**, 297–303. (doi:10.1016/0009-2614(90)85614-I)
6 Levitt, M. H. 1996 Composite pulses. In *Encyclopedia of nuclear magnetic resonance* (eds D. M. Grant & R. K. Harris), pp. 1396–1411. New York, NY: Wiley.
7 Berry, M. V. 1984 Quantal phase factors accompanying adiabatic changes. *Proc. R. Soc. Lond. A* **392**, 45–57. (doi:10.1098/rspa.1984.0023)
8 Simon, B. 1983 Holonomy, the quantum adiabatic theorem, and Berry's phase. *Phys. Rev. Lett.* **51**, 2167–2170. (doi:10.1103/PhysRevLett.51.2167)
9 Suter, D., Chingas, G. C., Harris, R. A. & Pines, A. 1987 Berry's phase in magnetic resonance. *Mol. Phys.* **61**, 1327–1340. (doi:10.1080/00268978700101831)
10 Du, J. *et al.* 2003 Observation of geometric phases for mixed states using NMR interferometry. *Phys. Rev. Lett.* **91**, 100403. (doi:10.1103/PhysRevLett.91.100403)
11 Zhang, Y., Tan, Y.-W., Stormer, H. L. & Kim, P. 2005 Experimental observation of the quantum Hall effect and Berry's phase in graphene. *Nature* **438**, 201–204. (doi:10.1038/nature04235)
12 Leek, P. J. *et al.* 2007 Observation of Berry's phase in a solid-state qubit. *Science* **318**, 1889–1892. (doi:10.1126/science.1149858)
13 Möttönen, M., Vartiainen, J. J. & Pekola, J. P. 2008 Experimental determination of the Berry phase in a superconducting charge pump. *Phys. Rev. Lett.* **100**, 177201. (doi:10.1103/PhysRevLett.100.177201)
14 Childs, A. M., Farhi, E. & Preskill, J. 2001 Robustness of adiabatic quantum computation. *Phys. Rev. A* **65**, 012322. (doi:10.1103/PhysRevA.65.012322)
15 De Chiara, G. & Palma, G. M. 2003 Berry phase for a spin 1/2 particle in a classical fluctuating field. *Phys. Rev. Lett.* **91**, 090404. (doi:10.1103/PhysRevLett.91.090404)
16 Lupo, C. & Aniello, P. 2009 Robustness of the geometric phase under parametric noise. *Phys. Scr.* **79**, 065012. (doi:10.1088/0031-8949/79/06/065012)
17 Jones, J. A., Vedral, V., Ekert, A. & Castagnoli, G. 2000 Geometric quantum computation using nuclear magnetic resonance. *Nature* **403**, 869–871. (doi:10.1038/35002528)
18 Falci, G., Fazio, R., Palma, G. M., Siewert, J. & Vedral, V. 2000 Detection of geometric phases in superconducting nanocircuits. *Nature* **407**, 355–358. (doi:10.1038/35030052)
19 Morton, J. J. L., Tyryshkin, A. M., Ardavan, A., Porfyrakis, K., Lyon, S. A. & Briggs, G. A. D. 2005 Measuring errors in single-qubit rotations by pulsed electron paramagnetic resonance. *Phys. Rev. A* **71**, 012332. (doi:10.1103/PhysRevA.71.012332)

20 Aharonov, Y. & Anandan, J. 1987 Phase change during a cyclic quantum evolution. *Phys. Rev. Lett.* **58**, 1593–1596. (doi:10.1103/PhysRevLett.58.1593)
21 Wu, H. *et al.* 2012 Geometric phase gates via adiabatic control using electron spin resonance. (http://arxiv.org/abs/1208.0555)
22 Suter, D., Mueller, K. T. & Pines, A. 1988 Study of the Aharonov–Anandan quantum phase by NMR interferometry. *Phys. Rev. Lett.* **60**, 1218–1220. (doi:10.1103/PhysRevLett.60.1218)
23 Morton, J. J. L., Tyryshkin, A. M., Ardavan, A., Benjamin, S. C., Porfyrakis, K., Lyon, S. A. & Briggs, G. A. D. 2006 Bang-bang control of fullerene qubits using ultrafast phase gates. *Nat. Phys.* **2**, 40–43. (doi:10.1038/nphys192)
24 Simmons, S. *et al.* 2011 Entanglement in a solid state spin ensemble. *Nature* **470**, 69–72. (doi:10.1038/nature09696)
25 Kwiat, P. & Chiao, R. 1991 Observation of a nonclassical Berry's phase for the photon. *Phys. Rev. Lett.* **66**, 588–591. (doi:10.1103/PhysRevLett.66.588)
26 Leek, P. J. *et al.* 2007 Observation of Berry's phase in a solid-state qubit. *Science* **318**, 1889–1892. (doi:10.1126/science.1149858)
27 Höfer, P. 1996 Multiple quantum pulsed ENDOR spectroscopy by time proportional phase increment detection. *Appl. Magn. Res.* **11**, 375–389. (doi:10.1007/BF03162234)
28 Scherer, W. & Mehring, M. 2008 Entangled electron and nuclear spin states in $^{15}N@C_{60}$: density matrix tomography. *J. Chem. Phys.* **128**, 052305. (doi:10.1063/1.2819310)
29 Filidou, V., Simmons, S., Karlen, S. D., Giustino, F., Anderson, H. L. & Morton, J. J. L. 2012 Ultrafast entangling gates between nuclear spins using photoexcited triplet states. *Nat. Phys.* **8**, 596–600. (doi:10.1038/nphys2353)
30 Schaffry, M., Lovett, B. & Gauger, E. 2011 Creating nuclear spin entanglement using an optical degree of freedom. *Phys. Rev. A* **84**, 032332. (doi:10.1103/PhysRevA.84.032332)
31 Hodges, J., Yang, J., Ramanathan, C. & Cory, D. 2008 Universal control of nuclear spins via anisotropic hyperfine interactions. *Phys. Rev. A* **78**, 010303(R). (doi:10.1103/PhysRevA.78.010303)
32 Zhang, Y., Ryan, C., Laflamme, R. & Baugh, J. 2011 Coherent control of two nuclear spins using the anisotropic hyperfine interaction. *Phys. Rev. Lett.* **107**, 170503. (doi:10.1103/PhysRevLett.107.170503)
33 Walther, P., Pan, J.-W., Aspelmeyer, M., Ursin, R., Gasparoni, S. & Zeilinger, A. 2004 De Broglie wavelength of a non-local four-photon state. *Nature* **429**, 158–161. (doi:10.1038/nature02552)
34 Afek, I., Ambar, O. & Silberberg, Y. 2010 High-NOON states by mixing quantum and classical light. *Science* **328**, 879–881. (doi:10.1126/science.1188172)
35 Mitchell, M. W., Lundeen, J. S. & Steinberg, A. M. 2004 Super-resolving phase measurements with a multiphoton entangled state. *Nature* **429**, 161–164. (doi:10.1038/nature02493)
36 Yurke, B. 1986 Input states for enhancement of fermion interferometer sensitivity. *Phys. Rev. Lett.* **56**, 1515–1517. (doi:10.1103/PhysRevLett.56.1515)
37 Holland, M. J. & Burnett, K. 1993 Interferometric detection of optical phase shifts at the Heisenberg limit. *Phys. Rev. Lett.* **71**, 1355–1358. (doi:10.1103/PhysRevLett.71.1355)
38 Roos, C. F., Chwalla, M., Kim, K., Riebe, M. & Blatt, R. 2006 'Designer atoms' for quantum metrology. *Nature* **443**, 316–319. (doi:10.1038/nature05101)
39 Kimble, H., Levin, Y., Matsko, A., Thorne, K. & Vyatchanin, S. 2001 Conversion of conventional gravitational-wave interferometers into quantum nondemolition interferometers by modifying their input and/or output optics. *Phys. Rev. D* **65**, 022002. (doi:10.1103/PhysRevD.65.022002)
40 Giovannetti, V., Lloyd, S. & Maccone, L. 2006 Quantum metrology. *Phys. Rev. Lett.* **96**, 010401. (doi:10.1103/PhysRevLett.96.010401)
41 Luis, A. & Sánchez-Soto, L. L. 1992 Breaking the standard quantum limit for interferometric measurements. *Opt. Commun.* **89**, 140–144. (doi:10.1016/0030-4018(92)90147-J)
42 Greenberger, D. M., Horne, M. A. & Zeilinger, A. 1989 Going beyond Bell's theorem. In *Bell's theorem, quantum theory, and conceptions of the universe* (ed. M. Kafatos), pp. 69–72. Dordrecht, The Netherlands: Kluwer.
43 Bollinger, J. J., Itano, W. M., Wineland, D. J. & Heinzen, D. J. 1996 Optimal frequency measurements with maximally correlated states. *Phys. Rev. A* **54**, R4649–R4652. (doi:10.1103/PhysRevA.54.R4649)

44 Jones, J. A., Karlen, S. D., Fitzsimons, J., Ardavan, A., Benjamin, S. C., Briggs, G. A. D. & Morton, J. J. L. 2009 Magnetic field sensing beyond the standard quantum limit using 10-spin NOON states. *Science* **324**, 1166–1168. (doi:10.1126/science.1170730)

45 Simmons, S., Jones, J. A., Karlen, S. D., Ardavan, A. & Morton, J. J. L. 2010 Magnetic field sensors using 13-spin cat states. *Phys. Rev. A* **82**, 022330. (doi:10.1103/PhysRevA.82.022330)

46 Morris, G. A. & Freeman, R. 1979 Enhancement of nuclear magnetic resonance signals by polarization transfer. *J. Am. Chem. Soc.* **101**, 760–762. (doi:10.1021/ja00497a058)

47 Modi, K., Cable, H., Williamson, M. & Vedral, V. 2011 Quantum correlations in mixed-state metrology. *Phys. Rev. X* **1**, 021022. (doi:10.1103/PhysRevX.1.021022)

48 Simmons, S. 2011 Creation and control of entanglement in condensed matter spin systems. PhD thesis, Oxford University, UK.

49 Tordrup, K., Negretti, A. & Molmer, K. 2008 Holographic quantum computing. *Phys. Rev. Lett.* **101**, 040501. (doi:10.1103/PhysRevLett.101.040501)

50 Afzelius, M., Simon, C., de Riedmatten, H. & Gisin, N. 2009 Multimode quantum memory based on atomic frequency combs. *Phys. Rev. A* **79**, 052329. (doi:10.1103/PhysRevA.79.052329)

51 Moiseev, S. A. & Kröll, S. 2001 Complete reconstruction of the quantum state of a single-photon wave packet absorbed by a Doppler-broadened transition. *Phys. Rev. Lett.* **87**, 173601. (doi:10.1103/PhysRevLett.87.173601)

52 Kraus, B., Tittel, W., Gisin, N., Nilsson, M., Kröll, S. & Cirac, J. I. 2006 Quantum memory for nonstationary light fields based on controlled reversible inhomogeneous broadening. *Phys. Rev. A* **73**, 020302. (doi:10.1103/PhysRevA.73.020302)

53 Hetet, G., Longdell, J. J., Alexander, A. L., Lam, P. K. & Sellars, M. J. 2008 Electro-optic quantum memory for light using two-level atoms. *Phys. Rev. Lett.* **100**, 023601. (doi:10.1103/PhysRevLett.100.023601)

54 Lauritzen, B., Minár, J., de Riedmatten, H., Afzelius, M., Sangouard, N., Simon, C. & Gisin, N. 2010 Telecommunication-wavelength solid-state memory at the single photon level. *Phys. Rev. Lett.* **104**, 080502. (doi:10.1103/PhysRevLett.104.080502)

55 Nunn, J., Reim, K., Lee, K. C., Lorenz, V. O., Sussman, B. J., Walmsley, I. A. & Jaksch, D. 2008 Multimode memories in atomic ensembles. *Phys. Rev. Lett.* **101**, 260502. (doi:10.1103/PhysRevLett.101.260502)

56 Hetet, G., Longdell, J. J., Sellars, M. J., Lam, P. K. & Buchler, B. C. 2008 Multimodal properties and dynamics of gradient echo quantum memory. *Phys. Rev. Lett.* **101**, 203601. (doi:10.1103/PhysRevLett.101.203601)

57 Wesenberg, J. H., Ardavan, A., Briggs, G. A. D., Morton, J. J. L., Schoelkopf, R. J., Schuster, D. I. & Mølmer, K. 2009 Quantum computing with an electron spin ensemble. *Phys. Rev. Lett.* **103**, 070502. (doi:10.1103/PhysRevLett.103.070502)

58 Wu, H. *et al.* 2010 Storage of multiple coherent microwave excitations in an electron spin ensemble. *Phys. Rev. Lett.* **105**, 140503. (doi:10.1103/PhysRevLett.105.140503)

59 Abe, E., Wu, H., Ardavan, A. & Morton, J. J. L. 2011 Electron spin ensemble strongly coupled to a three-dimensional microwave cavity. *Appl. Phys. Lett.* **98**, 251108. (doi:10.1063/1.3601930)

60 Schuster, D. I. *et al.* 2010 High-cooperativity coupling of electron-spin ensembles to superconducting cavities. *Phys. Rev. Lett.* **105**, 140501. (doi:10.1103/PhysRevLett.105.140501)

61 Kubo, Y. *et al.* 2010 Strong coupling of a spin ensemble to a superconducting resonator. *Phys. Rev. Lett.* **105**, 140502. (doi:10.1103/PhysRevLett.105.140502)

62 Rabl, P., DeMille, D., Doyle, J. M., Lukin, M. D., Schoelkopf, R. J. & Zoller, P. 2006 Hybrid quantum processors: molecular ensembles as quantum memory for solid state circuits. *Phys. Rev. Lett.* **97**, 033003. (doi:10.1103/PhysRevLett.97.033003)

63 Tordrup, K. & Molmer, K. 2008 Quantum computing with a single molecular ensemble and a Cooper-pair box. *Phys. Rev. A* **77**, 020301. (doi:10.1103/PhysRevA.77.020301)

64 Morton, J. J. L. & Lovett, B. W. 2011 Hybrid solid-state qubits: the powerful role of electron spins. *Annu. Rev. Condens. Matter Phys.* **2**, 189–212. (doi:10.1146/annurev-conmatphys-062910-140514)

65 Kubo, Y. *et al.* 2011 Hybrid quantum circuit with a superconducting qubit coupled to a spin ensemble. *Phys. Rev. Lett.* **107**, 220501. (doi:10.1103/PhysRevLett.107.220501)